Strong On-Chip Microwave Photon–Magnon Coupling Using Ultralow-Damping Epitaxial $Y_3Fe_5O_{12}$ Films at 2 Kelvin

*Side Guo, Daniel Russell, Joseph Lanier, Haotian Da, P. Chris Hammel, and Fengyuan Yang**

Department of Physics, The Ohio State University, Columbus, OH 43210, USA

ABSTRACT. $Y_3Fe_5O_{12}$ is arguably the best magnetic material for magnonic quantum information science (QIS) because of its extremely low damping. We report ultralow damping at 2 K in epitaxial $Y_3Fe_5O_{12}$ thin films grown on a diamagnetic $Y_3Sc_2Ga_3O_{12}$ substrate that contains no rare-earth elements. Using these ultralow damping YIG films, we demonstrate for the first time strong coupling between magnons in patterned YIG thin films and microwave photons in a superconducting Nb resonator. This result paves the road towards scalable hybrid quantum systems that integrate superconducting microwave resonators, YIG film magnon conduits, and superconducting qubits into on-chip QIS devices.

Key words: YIG epitaxial films, ultralow damping, magnon-photon coupling, on-chip hybrid quantum systems, superconducting microwave resonators.

Introduction

$Y_3Fe_5O_{12}$ (YIG) is a well-known ferrimagnetic insulator with extremely low magnetic damping, which makes it one of the best materials for fundamental studies and potential applications in magnonics, spintronics, and QIS.[1-9] To date, mm-scale YIG single-crystal spheres have been the material of choice for cavity magnonics[10-12] and coherently coupling

magnons to superconducting qubits[4] as well as for quantum sensing.[4,7,12,13] For QIS applications that require scalable on-chip integration, ultralow-damping magnetic films, which can be patterned and integrated in hybrid quantum systems, are highly desired. However, there is a major barrier for using YIG thin films in QIS because epitaxial YIG films are mostly grown on $Gd_3Ga_5O_{12}$ (GGG) or other garnet substrates containing rare-earth elements, which induce excessive damping loss in YIG films across the interface at low temperatures.[14] If this substrate-induced damping enhancement can be eliminated while maintaining high YIG film quality, it will enable scalable on-chip QIS devices based on ultralow-damping YIG films operating at mK temperatures.

Previously, we have shown that a diamagnetic epitaxial buffer layer of $Y_3Sc_{2.5}Al_{2.5}O_{12}$ can effectively separate the magnetic coupling between the YIG film and GGG substrate, resulting in much improved damping at low temperatures.[15] Here, we demonstrate the growth of YIG epitaxial films on a new diamagnetic $Y_3Sc_2Ga_3O_{12}$ (YSGG) single-crystal substrate containing no rare-earth elements, which exhibit extremely low damping that decreases rapidly with temperature below 5 K. By integrating patterned YIG epitaxial films on YSGG with superconducting Nb coplanar waveguide (CPW) microwave resonators, we observe strong coupling between microwave photons and magnons at 2 K.

Results and discussion

YIG thin films (bulk lattice constant a = 12.376 Å) are epitaxially grown on YSGG (111) substrates (a = 12.426 Å) using off-axis sputtering[16] with a 0.4% tensile strain on the YIG film. The crystalline quality of the YIG/YSGG films is characterized by X-ray diffraction (XRD) and X-ray reflectivity (XRR), as shown in Figs. 1a and 1b, respectively. The clear Laue oscillations of the YIG (444) peak indicate highly coherent crystalline ordering. The XRR fringes reveal the film thickness (30 nm) and low interfacial and surface roughness. Due to the 0.4% lattice mismatch between YIG and YSGG, thick YIG films (e.g., 100 nm) on YSGG is

susceptible to strain relaxation by incorporating defects. Meanwhile, for thinner YIG films (e.g., <10 nm), the influence of the surface and interface on damping can be more prominent. As a result, we choose an intermediate YIG film thickness of 30 nm for this study.[16]

Broadband ferromagnetic resonance (FMR) measurement is performed on a YIG(30 nm)/YSGG(111) film at various temperatures (T) between 2 and 300 K, as described previously.[15] We obtain FMR absorption spectra as a function of an in-plane magnetic field at various microwave frequencies (f) and temperatures. Figure 2a shows a representative derivative FMR spectrum at T = 2 K and f = 4.3 GHz. The resonance field H_r and linewidth ΔH are extracted from fitting the FMR spectrum using $y = [A - B(H - H_r)]/[(H - H_r)^2 + (\Delta H/2)^2]^2$, where A and B are the symmetric and antisymmetric amplitudes of the lineshape, respectively. From Fig. 2a, we obtain H_r = 710 Oe and ΔH = 13.2 Oe ($\sqrt{3}\times$ of peak-to-peak linewidth of 7.6 Oe).

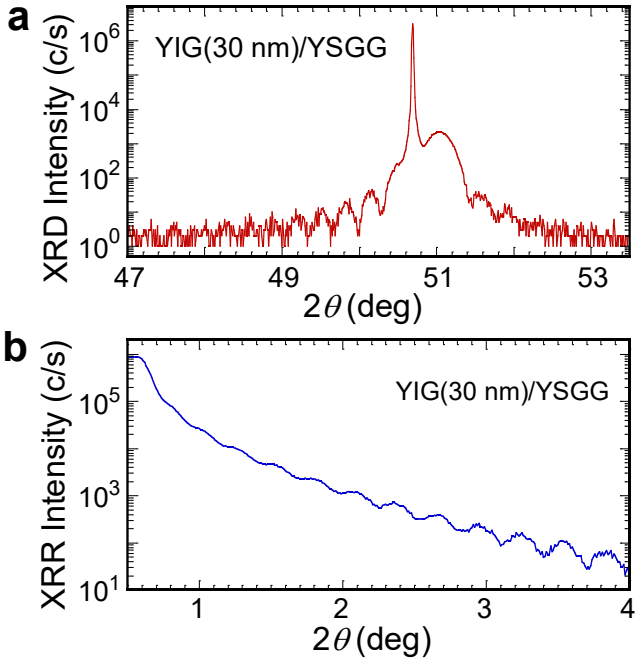

Figure 1. **X-ray diffraction results of YIG films. a**, $2\theta/\omega$ XRD scan and **b**, XRR scan of a YIG(30 nm) epitaxial film grown on YSGG (111) substrate, indicating the high crystalline quality of the YIG film.

We also measure the frequency-dependent FMR absorption at 2 K with a fixed in-plane field of 710 Oe using a vector network analyzer (VNA), as shown in Fig. 2b. The resonance

frequency f_r and linewidth Δf are extracted from fitting the spectrum with a Lorentzian function $y = A/[(f - f_r)^2 + (\Delta f/2)^2]$. The obtained f_r = 4.307 GHz and Δf = 36.3 MHz agree well with the field linewidth ΔH = 13.2 Oe as related by the gyromagnetic ratio of free electron, $\gamma/2\pi \approx 2.8$ MHz/G, where 36.3 MHz corresponds to 13.0 Oe.

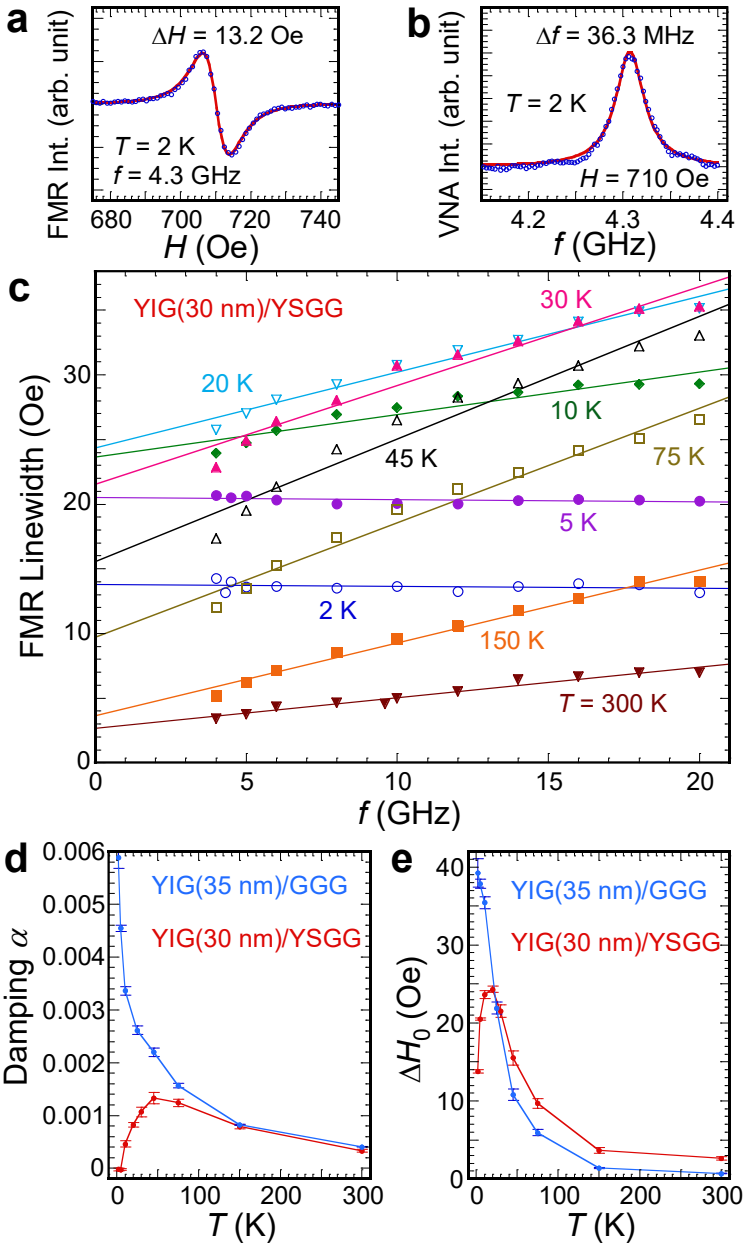

Figure 2. **FMR measurements of a YIG(30 nm)/YSGG film. a**, Field-dependent derivative FMR spectrum at 2 K driven by a microwave frequency of 4.3 GHz. **b**, Frequency-dependent FMR spectrum at 2 K with an in-plane field of 710 Oe. **c**, Frequency dependence of FMR linewidth at different temperatures, from which the damping constant and inhomogeneous broadening are obtained by linear fitting. Temperature dependence of **d** damping and **e** inhomogeneous broadening ΔH_0 for the YIG(30 nm)/YSGG film (red) and a conventional YIG(35 nm)/GGG film (blue). The error bars are from the linear fitting in **c**.

Figure 2c shows the extracted field linewidths of the YIG(30 nm)/YSGG film as a function of frequency at T = 2 to 300 K. As temperature decreases from 300 K, the linewidth and the slope of their frequency dependence increase and peak at 20-30 K, after which both ΔH and the slope decrease quickly down to 2 K (limited by our PPMS). This behavior agrees with the slow-relaxation theory in YIG,[17-19] where the existence of rare-earth impurities in YIG induces a significant enhancement of relaxation at temperatures of 10's K. At temperatures below this regime, the linewidth and the slope decrease significantly.

According to the Landau-Lifshitz-Gilbert (LLG) equation,[20] the FMR linewidth is linearly dependent on the microwave frequency with the slope determined by the phenomenological Gilbert damping coefficient (α): $\Delta H = 4\pi\alpha f/\gamma + \Delta H_0$, where ΔH_0 is the inhomogeneous broadening which is generally attributed to magnetic nonuniformity[21] and surface defects.[22] We note that the LLG equation is a simplified theory and does not explain the nonlinearity observed in the frequency dependence of ΔH, particularly at 10's K, which requires additional contributions such as the slow-relaxation mechanism. Nonetheless, our YIG/YSGG films' linewidth vs. frequency data shows a reasonably good linear dependence, especially near the two ends of the temperature window of 2-300 K, justifying the use of phenomenological damping coefficient α extracted from the LLG equation as a figure of merit. Meanwhile, the significantly reduced linewidths in YIG/YSGG films as compared to YIG/GGG films (see Figs. 2d and 2e) provide solid evidence for improvement of YIG damping behavior at cryogenic temperatures.

We fit the linewidth vs. frequency data in Fig. 2c using the LLG equation and extract damping α and inhomogeneous broadening ΔH_0 for each temperature, as shown in Figs. 2d and 2e, respectively. The damping starts at a very low value of $\alpha = 3.3 \times 10^{-4}$ at room temperature and increases as temperature drops. After reaching a peak of $\alpha = 1.3 \times 10^{-3}$ at 45 K, the damping decreases quickly at lower temperatures. Remarkably, the FMR linewidths are essentially

frequency independent at 5 and 2 K, indicating an essentially zero damping according to the LLG equation. This is in clear contrast with the significantly degraded α and ΔH_0 of a conventional YIG(35 nm) film grown on GGG, as shown in Figs. 2d and 2e for comparison,[15] which monotonically increase with decreasing temperature. We note that our YIG/YSGG films still have larger linewidths than YIG bulk crystals,[19] which can be attributed to the increased contribution from scattering at the surface and interface in very thin films.

Figure 2 shows a rapid decrease of linewidth below 10 K in our YIG/YSGG films, which can potentially lead to even narrower linewidths at sub-Kelvin temperatures. It should be pointed out that at such low temperatures, both YIG bulk single crystals[12] and YIG films with GGG substrate mechanically removed[23] are subject to relaxation arising from two-level systems, resulting in saturation of linewidth at very low temperatures. The linewidth of YIG/YSGG films at sub-Kelvin temperature range requires further investigation.

The extremely low damping of the YIG epitaxial films on diamagnetic YSGG substrates at very low temperatures is highly promising for QIS studies. As an initial step in this regard, we integrate the YIG/YSGG films with superconducting resonators for the study of coupling between magnons in a YIG film and microwave photons emitted by a superconducting CPW resonator. First, we pattern a YIG(30 nm)/YSGG film into 10-μm wide strips using photolithography and Ar ion milling. Then, 300-nm thick Nb resonators are deposited by sputtering on the YSGG substrate with photolithography patterns followed by lift-off such that the YIG strips lie within the gaps of the CPW resonators.

The microwave resonator design includes a main bus channel which is capacitively coupled to two resonators, as shown in Fig. 3a. The two resonators are 13- and 13.5-mm long with both ends open-circuit, so they resonate with half-wavelength standing waves, as determined by $f_r = c/2l\sqrt{\epsilon_{\text{eff}}}$, where c is the speed of light, l is the length of the resonator, and ϵ_{eff} is the average dielectric constant of vacuum and YSGG substrate. The center conductor

of the CPW resonators is 20-μm wide with a spacing gap of 15-μm from the group conductor on either side. A YIG strip is located within a gap of each resonator near the middle of the resonator length, as shown in the insets of Fig. 3a, which enables the magnetic field component of the resonating microwave to drive the FMR of the YIG strip. We fabricate two such devices with a total of four Nb resonators coupled to four YIG strips with 10-μm width and lengths of 300, 600, 900, and 1200 μm. In addition, we fabricate another such device with two Nb resonators on YSGG without YIG strips as a reference sample. The devices are mounted on a home-made sample holder and wire-bonded as shown in the insets of Fig. 3a, which is loaded into the PPMS and cooled down to 2 K.

Figure 3b shows the transmission spectrum (S21) of a device with two Nb resonators and no YIG, which exhibits two sharp dips at f = 4.203 and 4.364 GHz, corresponding to the resonances of the 13.5- and 13-mm resonators, with high quality factors (Q) of 5,380 and 5,670, respectively. It is noted that the measured resonance frequency ratio of (4.364 GHz)/(4.203 GHz) = 1.0383 is almost identical to the length ratio of (13.5 mm)/(13 mm) = 1.0385, validating the resonator design and fabrication.

Figure 3c compares the transmission spectra of a bare Nb resonator (no YIG) and a Nb resonator coupled to a 10 × 1200 μm^2 YIG strip at zero field or in the presence of an in-plane magnetic field of 550 Oe applied along the long axis of the YIG strip. Figure 3d shows similar spectra for a Nb resonator coupled to a 10 × 600 μm^2 YIG strip. All Nb resonators with or without coupling to YIG strips exhibit high quality factors between 4,000 and 8,000 at zero magnetic field. To evaluate the performance of the Nb resonators in a magnetic field needed for strong microwave photon-magnon coupling, we apply an in-plane field of 550 Oe, which lowers Q by a factor of ~2×, although the quality factor remains high (>2,000). This behavior together with shift of resonance frequency due to the applied field and coupling to YIG are commonly seen in other microwave photon–magnon coupling reports.[24,25]

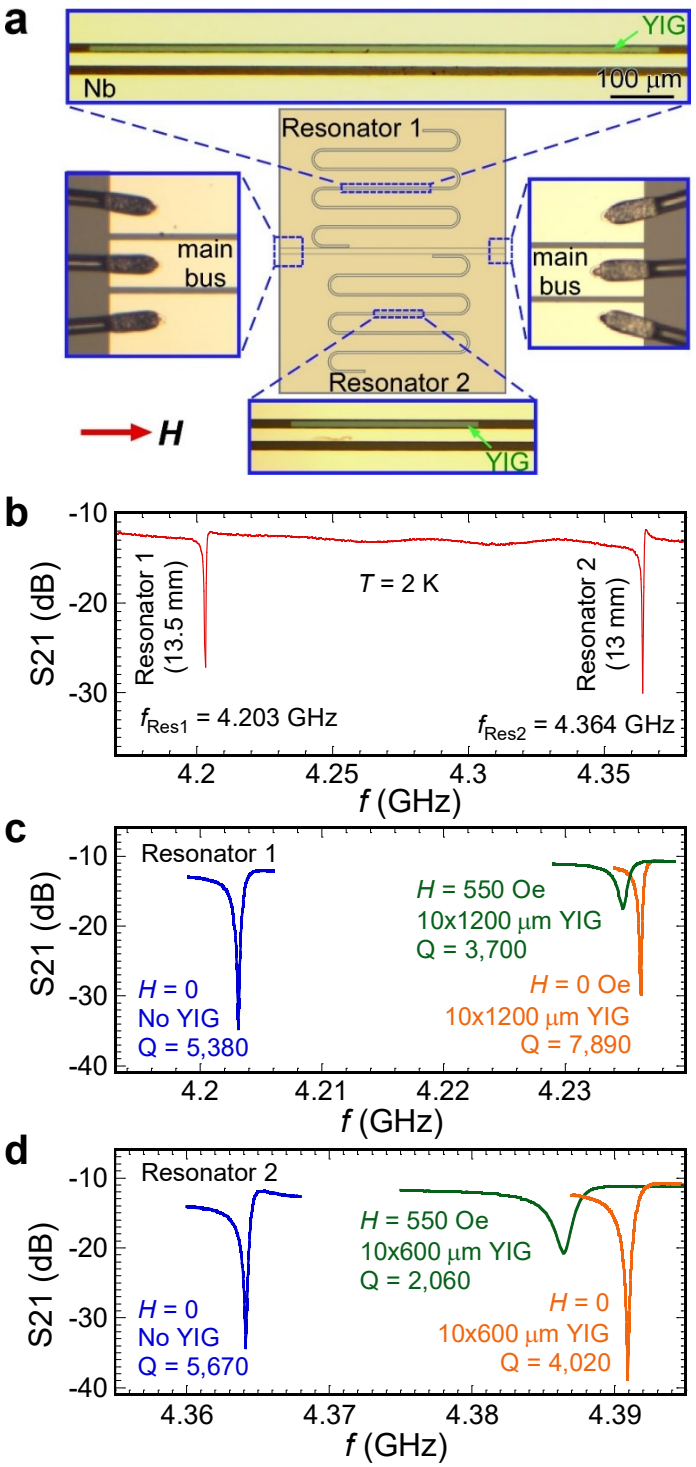

Figure 3. **Microwave transmission of Nb CPW resonators with or without YIG strips and magnetic field at 2 K. a**, Schematic of Nb resonator device with YIG strips placed within their gaps. The size of the whole device is 3.5 × 4.4 mm^2. The lengths of the two Nb resonators are 13 mm and 13.5 mm. Insets: optical microscope images of selected areas with the same magnification. The YIG strips shown (color contrast augmented) are 10 × 900 μm^2 (top) and 10 × 300 μm^2 (bottom). **b**, Microwave transmission (S21) spectrum of two Nb resonators without a YIG strip in their gaps. The two sharp dips (resonances) at 4.364 and 4.203 GHz correspond to the resonance frequencies of the 13 mm and 13.5 mm resonators, respectively. **c**, Microwave transmission spectra of the 13.5 mm resonators without YIG at zero field (blue), with a 10 × 1200 μm^2 YIG strip at zero field (orange), and with a 10 × 1200 μm^2 YIG strip in

the presence of a 550 Oe in-plane magnetic field (green) as illustrated in **a**. **d**, Microwave transmission spectra of the 13 mm resonators without YIG at zero field (blue), with a 10 × 600 μm^2 YIG strip at zero field (orange), and with a 10 × 600 μm^2 YIG strip at 550 Oe (green).

Such resonator-ferromagnet hybrid systems can be modeled as a macrospin coupled to an *LC* resonator by the radio-frequency (rf) magnetic field component b_{rf}.[24] The eigenfrequencies of this system can be calculated as,

$$\omega_{\pm} = \big(\omega_r + \omega_m(H)\big)/2 \pm \sqrt{(\omega_m(H) - \omega_r)^2 + 4g^2}/2, \quad (1)$$

where ω_{r} is the resonance frequency of a standalone microwave resonator, $\omega_m(H)$ is the standalone ferromagnet's FMR frequency (dependent on the applied field H), and g is the total photon-magnon coupling strength. The total coupling strength scales with the number of spins N in the ferromagnet as $g = g_s\sqrt{N}$, where g_s is the coupling strength between microwave photons and individual spins in the ferromagnet, which depends on the device design and microwave magnetic field strength b_{rf} at the ferromagnet. Note that the number of spins here is a net value due to YIG's ferrimagnetism.

We perform field-dependent transmission measurement on the 13- and 13.5-mm Nb resonators to quantify their coupling strength to the 10 × 300 μm^2, 10 × 600 μm^2, 10 × 900 μm^2, and 10 × 1200 μm^2 YIG strips. Figures 4a-4d show the microwave transmission of the four resonator-YIG hybrid devices as a function of field and frequency measured at 2 K. The anticrossing features in the plots are the signatures of microwave photon-magnon coupling, where YIG's FMR frequency $\omega_{\mathrm{m}}(H) = \gamma\sqrt{H(H + 4\pi M_{\mathrm{eff}})}$ (M_{eff} : effective saturation magnetization) meets the microwave resonator's resonance frequency ω_r, and the degeneracy is lifted. Each plot has the same frequency and field scales for direct comparison of the anticrossing opening.

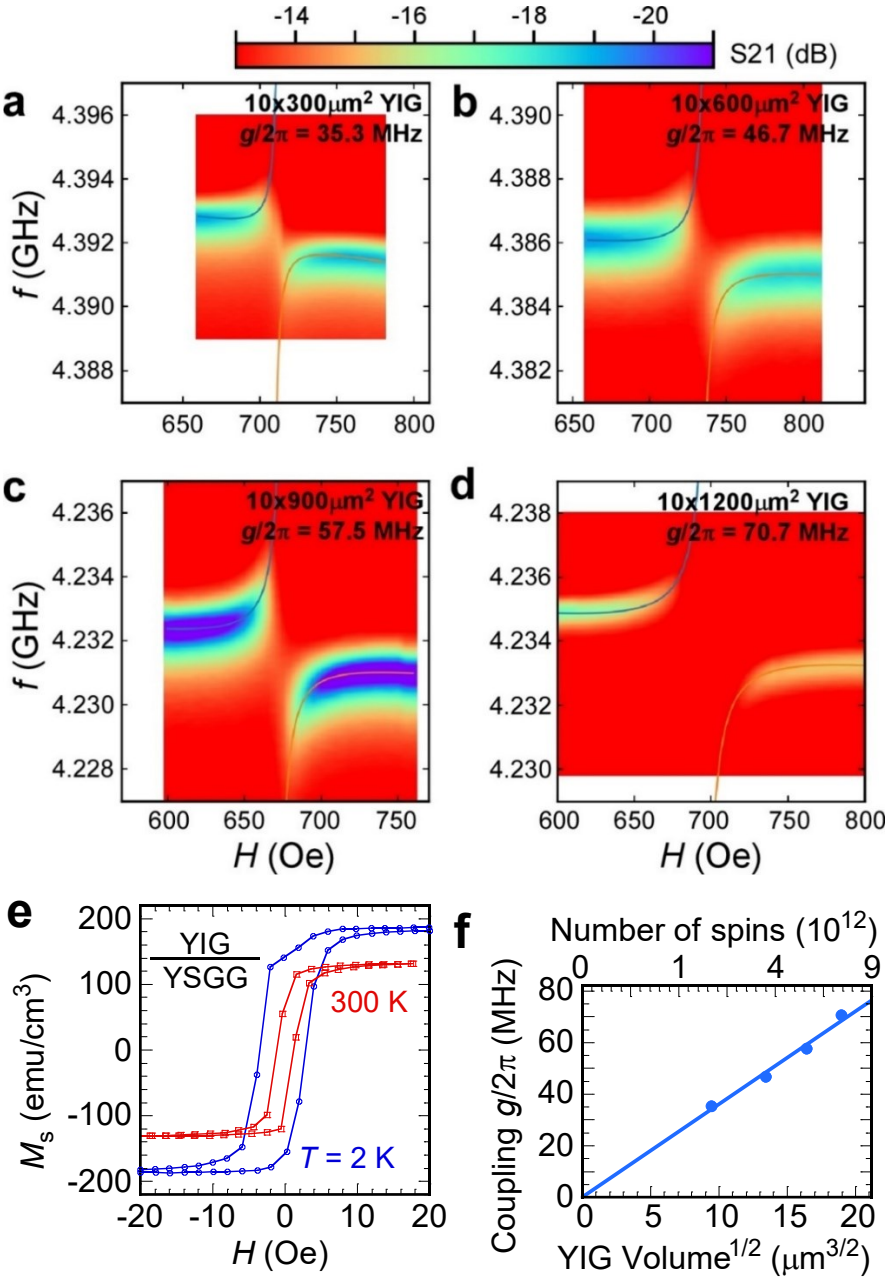

Figure 4. Microwave photon-magnon coupling in Nb resonator-YIG(30 nm) hybrid structures on YSGG. a-d, Microwave transmission in Nb resonators coupled to YIG strips of **a**, 10 × 300 μm^2, **b**, 10 × 600 μm^2, **c**, 10 × 900 μm^2, and **d**, 10 × 1200 μm^2, as a function of microwave frequency and in-plane magnetic field at 2 K. **e**, Magnetic hysteresis loops of a YIG(30 nm)/YSGG film at 2 and 300 K. **f**, Coupling strength between microwave photons and magnons in the YIG films as a function of the square root of the magnetic volume as well as the number of spins in YIG.

We point out that different aspect ratios of the YIG strips can give rise to different demagnetizing factors, which slightly shift $\omega_m(H)$. However, this shift is smaller than 1 Oe over the field-frequency range of interest and thus is ignored here. We fit the anticrossing features with Eq. (1) and extract the coupling strength g which is dependent on the magnetic

volume and the number of spins N. For the fitting, a background linearly dependent on the field is added to Eq. (1) to account for the field-induced microwave resonator frequency shift.

To determine the number of spins in a YIG strip, we measure magnetic hysteresis loops for the YIG(30 nm)/YSGG film using a superconducting quantum interference device (SQUID) magnetometer at 2 and 300 K, as shown in Fig. 4e. The saturation magnetization is determined to be M_S = 180 emu/cm^3 at 2 K and 131 emu/cm^3 at 300 K. The hysteresis loops remain largely square with a small coercivity of 1.1 and 3.1 Oe at 300 and 2 K, respectively, corroborating the high magnetic uniformity at both room and cryogenic temperatures.

Figure 4f shows the linear dependence of coupling strength $g/2\pi$ on the square root of both the YIG volume and the number of spins. From Fig. 2b, the decay rate $\kappa_\mathrm{m}/2\pi$ of YIG's resonance mode near 4.3 GHz at 2 K and H = 710 Oe is determined to be 36.3 MHz. Next, the decay rate $\kappa_\mathrm{r}/2\pi$ of the Nb resonator is estimated to be 2.13 MHz based on the transmission linewidth of the resonator coupled to the 10 × 600 μm^2 YIG strip at H = 550 Oe as shown in Fig. 3d. Thus, the cooperativity for the 10 × 600 μm^2 YIG is calculated to be $g^2/(\kappa_r\kappa_m) \approx$ 28.2, showing that the coupling strength is much stronger than the decay rates of individual components, which is required for coherent coupling.

Using M_S = 180 emu/cm^3 at 2 K for the YIG/YSGG film, we determine the average coupling strength to an individual spin to be $g_s/2\pi$ = 25.1 Hz. This coupling strength $g_s/2\pi$ is comparable to other reports on microwave photon-magnon coupling using ferromagnetic metals[24-26] and similar CPW resonator-ferromagnet structures. Considering that the microwave magnetic field in the gap of a CPW (where our YIG strip is located) is weaker than that for a ferromagnet directly on top (or underneath) the superconducting center conductor channel, one can achieve stronger microwave photon-magnon coupling by positioning the YIG strip near a stronger microwave magnetic field or utilizing resonator designs such as lumped-element *LC* resonator, which can provide far stronger coupling strength.[24]

This work provides the first demonstration that ultralow-damping YIG epitaxial films on YSGG can be integrated with superconductor resonators to achieve strong microwave photon-magnon coupling at few Kelvin temperatures. Such ultralow-damping YIG films offer clear advantages (in terms of decay rate) over metallic ferromagnets for on-chip hybrid quantum systems that incorporate magnonic conduits, microwave superconductor resonators, and superconductor qubits for QIS applications that operate in the mK regime.

Conclusion

In summary, we demonstrate the growth of high-quality epitaxial YIG thin films on diamagnetic YSGG substrate, which exhibit narrow FMR linewidth and extremely low damping at 2 K. We couple these YIG films to superconducting Nb resonators to create hybrid structures that achieve strong microwave photon-magnon coupling. This work demonstrates the potential power of ultralow-damping YIG films for scalable, integrated QIS applications at low temperatures.

Methods

The YSGG(111) crystal substrates are purchased from MTI Corporation and have a bulk lattice constant of a = 12.466 Å, which causes a 0.72% tensile strain in the YIG film (bulk a = 12.376 Å). The YIG films are deposited with a substrate temperature of 675 ℃ and in a 11.5 mTorr of Ar+1%O_2 gas. High phase-purity YIG nanometer-sized powders synthesized using sol-gel method is cold-pressed into the YIG sputtering target used for magnetron sputtering deposition. XRD and XRR on the YIG films are performed using Rigaku Smarlab X-ray diffractometor, with Cu K-alpha$_1$ line (λ=1.5406 Å). Nb films are deposited at room temperature using magnetron sputtering, too.

Broadband FMR measurement of YIG/YSGG(111) film is performed in a Dynacool Physical Property Measurement System (PPMS) from Quantum Design, which provides

temperature control and in-plane magnetic field sweeping. External electronics are Keithley Model 6221 AC and DC Current Source (in-plane magnetic field modulation), Keysight N5183B MXG X-Series Microwave Analog Signal Generator (magnetic resonance driving) and Stanford Research SR830 DSP Dual Phase Lock-In Amplifier (microwave transmission pickup). YIG/YSGG film is mounted on a CPW probe designed by Quantum Design.

Frequency spectrum of microwave transmission is performed using Rhode & Schwarz ZNLE14 VNA. Two-port transmission measurements use an output power of -40 dBm without attenuators or amplifiers, where each result spectrum is averaged over 40 scans.

The photolithography uses Microposit S1813 photo resist and MicroChem LOR 3A lift-off resist. Exposure of resist by Heidelberg μPG501 Maskless Aligner is followed by Microposit MF-319 developer.

SQUID Magnetometry is performed in a Quantum Design MPMS 3 SQUID Magnetometer that allows temperature control.

Acknowledgement

This work was primarily supported by the Center for Emergent Materials: an NSF MRSEC under award number DMR-2011876. D.R. acknowledges partial support from the National Science Foundation under award number DMR-2225646 (YIG film growth and X-ray characterizations).

Corresponding Author: Fengyuan Yang. Email: yang.1006@osu.edu

Author Contributions

SG was responsible in the experiment design, setting up measurement and was a major contributor in the data analysis and manuscript writing. DR performed XRD and XRR on the YIG/YSGG thin film. JL performed the SQUID measurement on the YIG/YSGG thin film. HD contributed to the photolithography step of device making and microwave resonator design exploration. PCH and FYY supervised the project. All authors read and approved the final

manuscript.

References:

1 Serga, A. A., Chumak, A. V. & Hillebrands, B. YIG magnonics. *J. Phys. D-Appl. Phys.* **2010**, 43, 264002.

2 Chumak, A. V., Vasyuchka, V. I., Serga, A. A. & Hillebrands, B. Magnon spintronics. *Nat. Phys.* **2015**, 11, 453-461.

3 Cornelissen, L. J., Liu, J., Duine, R. A., Youssef, J. B. & van Wees, B. J. Long-distance transport of magnon spin information in a magnetic insulator at room temperature. *Nat. Phys.* **2015**, 11, 1022-1026.

4 Tabuchi, Y., Ishino, S., Noguchi, A., Ishikawa, T., Yamazaki, R., Usami, K. & Nakamura, Y. Coherent coupling between a ferromagnetic magnon and a superconducting qubit. *Science* **2015**, 349, 405.

5 Lachance-Quirion, D., Tabuchi, Y., Gloppe, A., Usami, K. & Nakamura, Y. Hybrid quantum systems based on magnonics. *Appl. Phys. Express* **2019**, 12, 070101.

6 Clerk, A. A., Lehnert, K. W., Bertet, P., Petta, J. R. & Nakamura, Y. Hybrid quantum systems with circuit quantum electrodynamics. *Nat. Phys.* **2020**, 16, 257-267.

7 Lachance-Quirion, D., Wolski, S. P., Tabuchi, Y., Kono, S., Usami, K. & Nakamura, Y. Entanglement-based single-shot detection of a single magnon with a superconducting qubit. *Science* **2020**, 367, 425.

8 Li, Y., Zhang, W., Tyberkevych, V., Kwok, W.-K., Hoffmann, A. & Novosad, V. Hybrid magnonics: Physics, circuits, and applications for coherent information processing. *J. Appl. Phys.* **2020**, 128, 130902.

9 Xu, Q., Cheung, H. F. H., Cormode, D. S., Puel, T. O., Yusuf, H., Chilcote, M., Flatté, M. E., Johnston-Halperin, E. & Fuchs, G. D. Strong photon-magnon coupling using a lithographically defined organic ferrimagnet. *arXiv:2212.04423* **2022**.

10 Zare Rameshti, B., Viola Kusminskiy, S., Haigh, J. A., Usami, K., Lachance-Quirion, D., Nakamura, Y., Hu, C.-M., Tang, H. X., Bauer, G. E. W. & Blanter, Y. M. Cavity magnonics. *Phys. Rep.* **2022**, 979, 1-61.

11 Li, Y., Yefremenko, V. G., Lisovenko, M., Trevillian, C., Polakovic, T., Cecil, T. W., Barry, P. S., Pearson, J., Divan, R., Tyberkevych, V., Chang, C. L., Welp, U., Kwok, W.-K. & Novosad, V. Coherent Coupling of Two Remote Magnonic Resonators Mediated by Superconducting Circuits. *Phys. Rev. Lett.* **2022**, 128, 047701.

12 Tabuchi, Y., Ishino, S., Ishikawa, T., Yamazaki, R., Usami, K. & Nakamura, Y. Hybridizing Ferromagnetic Magnons and Microwave Photons in the Quantum Limit. *Phys. Rev. Lett.* **2014**, 113, 083603.

13 Wolski, S. P., Lachance-Quirion, D., Tabuchi, Y., Kono, S., Noguchi, A., Usami, K. & Nakamura, Y. Dissipation-Based Quantum Sensing of Magnons with a Superconducting Qubit. *Phys. Rev. Lett.* **2020**, 125, 117701.

14 Jermain, C. L., Aradhya, S. V., Reynolds, N. D., Buhrman, R. A., Brangham, J. T., Page, M. R., Hammel, P. C., Yang, F. Y. & Ralph, D. C. Increased low-temperature damping in yttrium iron garnet thin films. *Phys. Rev. B* **2017**, 95, 174411.

15 Guo, S. D., McCullian, B., Hammel, P. C. & Yang, F. Y. Low damping at few-K temperatures in $Y_3Fe_5O_{12}$ epitaxial films isolated from $Gd_3Ga_5O_{12}$ substrate using a diamagnetic $Y_3Sc_{2.5}Al_{2.5}O_{12}$ spacer. *J. Magn. Magn. Mater.* **2022**, 562, 169795.

16 Yang, F. Y. & Hammel, P. C. Topical review: FMR-Driven Spin Pumping in $Y_3Fe_5O_{12}$-Based Structures. *J. Phys. D: Appl. Phys.* **2018**, 51, 253001.

17 Maier-Flaig, H., Klingler, S., Dubs, C., Surzhenko, O., Gross, R., Weiler, M., Huebl, H. & Goennenwein, S. T. B. Temperature-dependent magnetic damping of yttrium iron garnet spheres. *Phys. Rev. B* **2017**, 95, 214423.
18 Seiden, P. E. Ferrimagnetic Resonance Relaxation in Rare-Earth Iron Garnets. *Phys. Rev.* **1964**, 133, A728-A736.
19 Spencer, E. G., LeCraw, R. C. & Clogston, A. M. Low-Temperature Line-Width Maximum in Yttrium Iron Garnet. *Phys. Rev. Lett.* **1959**, 3, 32-33.
20 Vonsovskii, S. V. *Ferromagnetic Resonance: The Phenomenon of Resonant Absorption of a High-Frequency Magnetic Field in Ferromagnetic Substances*. (Pergamon, 1966).
21 Schlömann, E. Inhomogeneous Broadening of Ferromagnetic Resonance Lines. *Phys. Rev.* **1969**, 182, 632-645.
22 Klingler, S., Maier-Flaig, H., Dubs, C., Surzhenko, O., Gross, R., Huebl, H., Goennenwein, S. T. B. & Weiler, M. Gilbert damping of magnetostatic modes in a yttrium iron garnet sphere. *Appl. Phys. Lett.* **2017**, 110, 092409.
23 Kosen, S., van Loo, A. F., Bozhko, D. A., Mihalceanu, L. & Karenowska, A. D. Microwave magnon damping in YIG films at millikelvin temperatures. *APL Mater.* **2019**, 7, 101120.
24 Hou, J. T. & Liu, L. Q. Strong Coupling between Microwave Photons and Nanomagnet Magnons. *Phys. Rev. Lett.* **2019**, 123, 107702.
25 Li, Y., Polakovic, T., Wang, Y.-L., Xu, J., Lendinez, S., Zhang, Z. Z., Ding, J. J., Khaire, T., Saglam, H., Divan, R., Pearson, J., Kwok, W.-K., Xiao, Z. L., Novosad, V., Hoffmann, A. & Zhang, W. Strong Coupling between Magnons and Microwave Photons in On-Chip Ferromagnet-Superconductor Thin-Film Devices. *Phys. Rev. Lett.* **2019**, 123, 107701.
26 Haygood, I. W., Pufall, M. R., Edwards, E. R. J., Shaw, J. M. & Rippard, W. H. Strong Coupling of an FeCo Alloy with Ultralow Damping to Superconducting Co-planar Waveguide Resonators. *Phys. Rev. Appl.* **2021**, 15, 054021.